Research Square

Preprints are preliminary reports that have not undergone peer review.
They should not be considered conclusive, used to inform clinical practice,
or referenced by the media as validated information.

Meteorological Conditions Associated with the 5 August 2025 Dharali Disaster in India

Rohit Thapliyal
Indian Institute of Technology Roorkee
Chander Singh Tomar
India Meteorological Department
Piyush Srivastava
piyush.srivastava@dm.iitr.ac.in

Indian Institute of Technology Roorkee

Research Article

Keywords: Debris flow, Uttarakhand, Western disturbance, Monsoon meteorology, Satellite rainfall estimation, Numerical weather prediction, Himalayan hazards, Thermodynamic instability

Posted Date: March 25th, 2026

DOI: https://doi.org/10.21203/rs.3.rs-9101402/v1

License: This work is licensed under a Creative Commons Attribution 4.0 International License.
Read Full License

Additional Declarations: No competing interests reported.

Version of Record: A version of this preprint was published at Meteorology and Atmospheric Physics on October 12th, 2026. See the published version at https://doi.org/10.1007/s00703-026-01214-y.

Meteorological Conditions Associated with the 5 August 2025 Dharali Disaster in India

Rohit Thapliyal[1,2], Chander Singh Tomar[2], Piyush Srivastava[1*]

[1] Centre of Excellence in Disaster Mitigation and Management, Indian Institute of Technology Roorkee, India

[2] Meteorological Centre, India Meteorological Department, Dehradun, India

***Corresponding author**

Prof. Piyush Srivastava

Centre of Excellence in Disaster Mitigation and Management,

Indian Institute of Technology Roorkee, India-247667

Abstract

On August 5, 2025, a catastrophic debris flow in the Khirgad stream, Uttarkashi district, Uttarakhand, caused extensive damage to life and infrastructure in Dharali and Harsil villages. This study presents a comprehensive meteorological analysis of the synoptic, dynamic, and thermodynamic conditions that contributed to this disaster. Multisource observational data, including surface and upper-air measurements, satellite imagery, numerical weather prediction models (IMD-GFS and WRF), and thermodynamic diagnostics, were analysed. The results indicate that moderate rainfall (~20 mm) was observed over Dharali on August 5, 2025, while extremely heavy precipitation occurred in the southern districts of Uttarakhand. The synoptic analysis showed an active monsoon trough north of its normal position with the eastern end running close to the Himalayan foothills, a mid-tropospheric trough running from northwest Uttar Pradesh to northeast Arabian Sea, and a quasistationary western disturbance. Thermodynamic analysis revealed an increase in precipitable water content and favourable atmospheric instability indices and a dynamic environment. Satellite-based rainfall estimation techniques showed considerable uncertainty, with GPM underestimating, IMSRA underestimating maxima, and HEM overestimating rainfall amounts. However, all the satellite estimates showed rainfall maxima over southern Uttarakhand and adjoining Uttar Pradesh. Both the IMD-GFS and WRF models captured the broad synoptic setting and provided fairly good guidance in the identification of the region of rainfall maxima. This study underscores that in the Higher Himalayan region, relatively moderate rainfall in the presence of favourable hydro- and geological settings can trigger devastating mass movements. There is a need for improved high-resolution rainfall estimation, enhanced representation of orographic effects in numerical models, and development of localized warning systems for hydrogeo-meteorological hazards in mountainous terrain.

Keywords: Debris flow, Uttarakhand, Western disturbance, Monsoon meteorology, Satellite rainfall estimation, Numerical weather prediction, Himalayan hazards, Thermodynamic instability

1. Introduction

The Indian Himalayan region is highly susceptible to hydrometeorological disasters, particularly during the southwest monsoon season, when orographic enhancement of rainfall, coupled with steep terrain and fragile geology, creates conditions conducive to landslides, debris flows, and flash floods (Dikshit et al., 2020; Martha et al., 2021). The state of Uttarakhand, situated in the Western Himalaya, experiences recurring devastating events, including the catastrophic floods of June 2013 and October 2021 that claimed many lives (Dube et al., 2014; Thapliyal & Singh, 2023). Understanding the meteorological precursors and atmospheric conditions associated with such events is crucial for improving prediction capabilities and early warning systems.

On the afternoon of August 5, 2025, a devastating debris flow originated in the Khirgad stream (also known as Kheer Gad) in Uttarkashi district, Uttarakhand, resulting in two confirmed fatalities and 67 persons reported missing. The event caused catastrophic damage to residential structures, commercial buildings, bridges, and road infrastructure in the villages of Dharali and Harsil. According to satellite analysis by the National Remote Sensing Centre (NRSC, 2025), the debris flow deposited a fan-shaped accumulation of sediment and debris covering approximately 20 hectares (750 m × 450 m) at Dharali village, located at the confluence of Kheer Gad and the Bhagirathi River. The satellite image of the affected area is shown in Fig. 1.

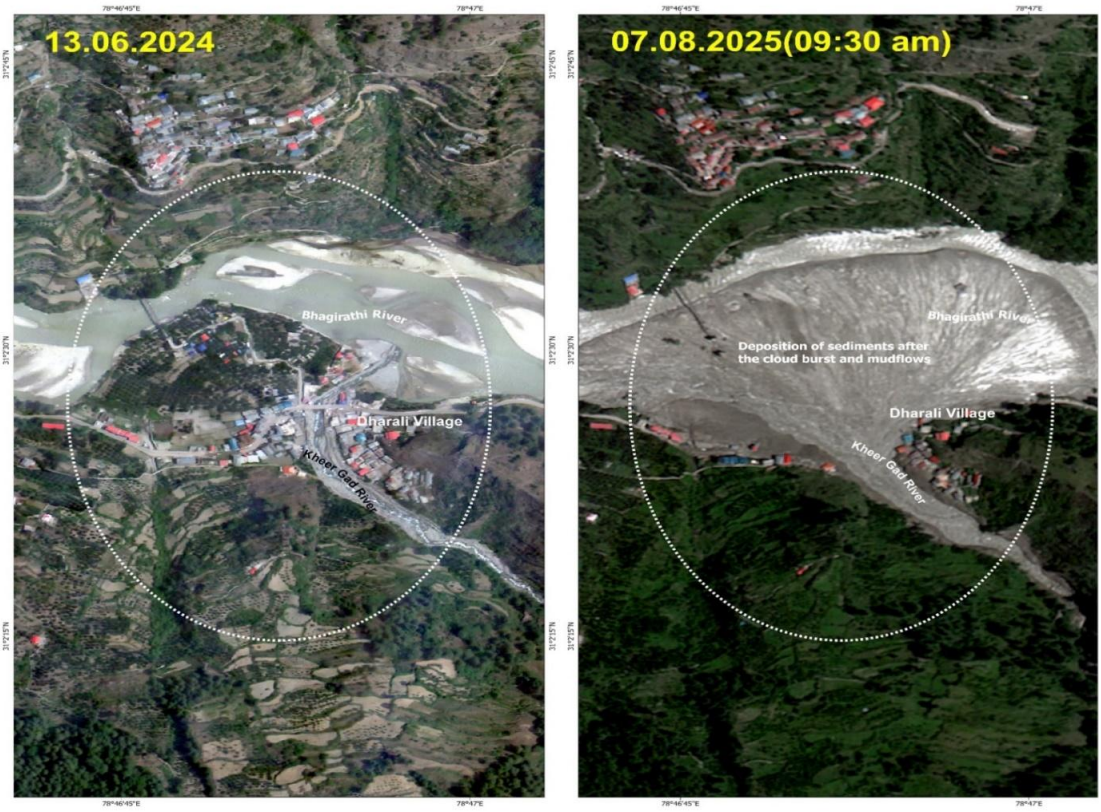


Fig 1: Pre- and postevent satellite images of Dharali, Uttarkashi district, Uttarakhand, India (Source: NRSC).

Uttarakhand's annual precipitation is dominated by the southwest monsoon (June-September), which contributes approximately 80% of the state's total annual rainfall of 1478 mm, with an average monsoon precipitation of 1162.7 mm (IMD, 2023). The Uttarkashi district typically receives rainfall comparable to the state average during monsoon months, varying from 2% above average in July to 8% below average in September. However, during the winter and premonsoon months (October-April), Uttarkashi receives 20-35% more precipitation than the state average due to the influence of western disturbances and extratropical weather systems that bring significant moisture from the Mediterranean and Caspian Sea regions (Dimri and Chevuturi, 2014; Hunt et al., 2018). The monthly average rainfall of the Uttarakhand and Uttarkashi districts is shown in Fig. 2.

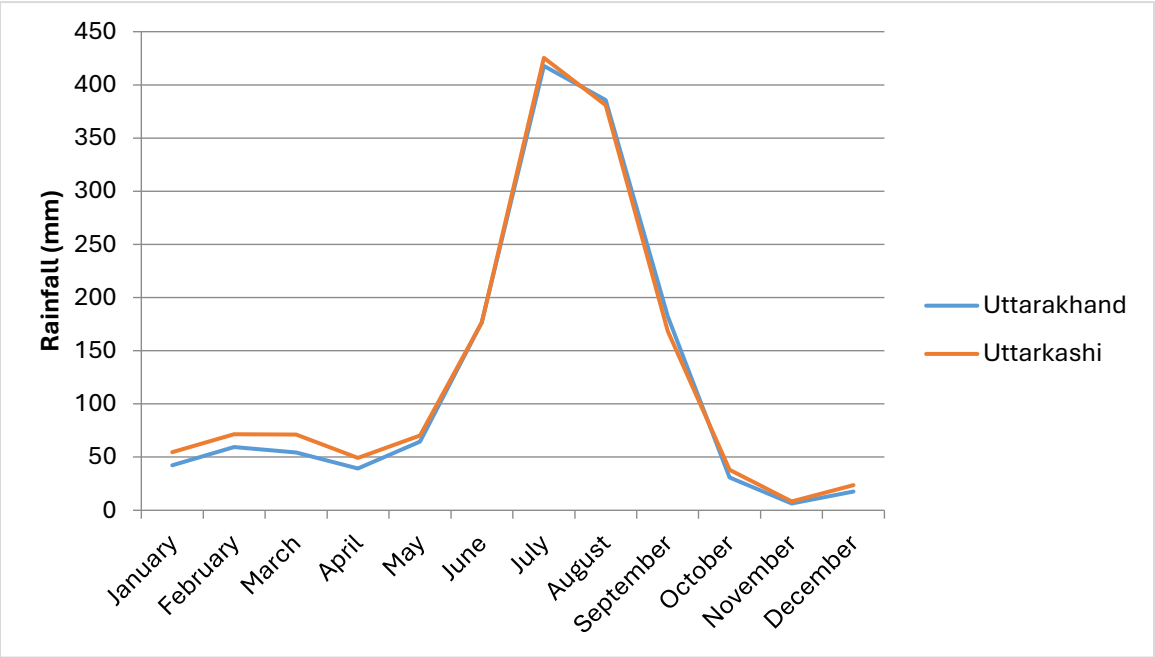


Fig 2: Monthwise average rainfall of the Uttarakhand and Uttarkashi districts.

Debris flows in mountainous regions result from complex interactions between meteorological forcings, hydrological responses, and geomorphological characteristics (Wieczorek et al., 2001; Iverson et al., 2000). Unlike events in lower elevation regions where extreme rainfall thresholds are typically required (Guzzetti et al., 2008), Himalayan mass movements can be triggered by relatively moderate precipitation due to the presence of unconsolidated glacial deposits, permafrost degradation, steep slopes, and high antecedent moisture conditions (Stoffel and Huggel, 2012; Allen et al., 2016). Climate change is further exacerbating these vulnerabilities through enhanced glacier retreat, permafrost thaw, and potential intensification of extreme precipitation events (Dimri et al., 2018).

The prediction of localized extreme rainfall events in complex mountainous terrain remains a significant challenge for numerical weather prediction (NWP) models due to inadequate representation of orographic processes, insufficient spatial resolution, and uncertainties in microphysical parameterizations (Norris et al., 2014; Chevuturi et al., 2015; Karki et al., 2018). Similarly, satellite-based rainfall estimation techniques face considerable uncertainties over mountainous regions due to terrain effects on radar reflectivity, warm rain processes, and challenges in relating cloud-top properties to surface precipitation (Shige et al., 2013; Kidd and Levizzani, 2011).

This study aims to provide a comprehensive meteorological analysis of the atmospheric conditions that led to the August 5, 2025 Dharali disaster. We examine the synoptic-scale atmospheric circulation patterns, mesoscale features, thermodynamic environment, and model forecast performance to (1) characterize the large-scale atmospheric setting and its evolution; (2) assess the performance of various rainfall estimation techniques; and (3) evaluate numerical model skill in predicting the event to understand why relatively moderate rainfall triggered such a catastrophic response in this high-altitude Himalayan setting. The findings will contribute to an improved understanding of Himalayan hydrometeorological disasters and support the development of enhanced forecasting and warning capabilities.

2. Study Area and Climatological Context

The Dharali-Harsil region is located in the Uttarkashi district of Uttarakhand in the Garhwal Himalaya, along the upper reaches of the Bhagirathi River, one of the primary headwater streams of the Ganges River. Dharali is situated at an altitude of 2520 m above the mean sea level. This high-altitude area is characterized by steep mountainous terrain, narrow valleys, and the presence of glacial and periglacial landforms. The region experiences a complex climate influenced by both monsoon circulation and mid-latitude westerly disturbances.

The Rudraprayag district in Uttarakhand experiences the highest average monsoon rainfall of approximately 1549 mm, while Uttarkashi receives amounts comparable to the state average. The temporal distribution of rainfall shows strong seasonality, with July and August being the wettest months, collectively contributing more than 800 mm of rainfall (more than 50% of the annual total rainfall). This concentrated precipitation during the monsoon season, combined with antecedent moisture from premonsoon rainfall, creates highly saturated soil and slope conditions that increase the susceptibility to mass movements.

3. Data and Methodology

3.1. Observational Data

Surface meteorological observations at 0300 UTC and upper-air radiosonde/radiowind (RS/RW) measurements at 0000 UTC from India Meteorological Department (IMD) stations were utilized for synoptic analysis. The upper-air data from Patiala station, located approximately 200 km southwest of Uttarkashi, were employed for atmospheric sounding and thermodynamic parameter calculation. According to GCOS guidelines, the area of representation for radiosonde stations is sufficiently large to provide representative upper-air conditions for the Uttarkashi region (Jones et

al., 2010). It is acknowledged that the mesoscale features in Uttarkashi district may not be fully captured by Patiala's upper-air data, introducing limitations to the study. However, this approach is consistent with operational practice in regions with sparse observational networks.

Rainfall data were obtained from a dense network comprising 140 Automatic Weather Stations (AWS), 49 Automatic Rain Gauges (ARG), and 71 Districtwise Rainfall Measuring Stations (DRMS) across Uttarakhand. For a detailed analysis of the Uttarkashi district, 15-minute interval data from 6 AWS locations and 24-hour accumulated rainfall from 7 DRMS and 5 non-DRMS stations were analysed to characterize the spatial and temporal distribution of precipitation.

3.2. Satellite Data

Multispectral satellite imagery from INSAT-3D was analysed, including visible channel, thermal infrared (TIR1-10.8 μm), cloud-top brightness temperature (CTBT), and derived products including upper-level divergence (ULD) and lower-level convergence (LLC). Water vapour channel winds were used to diagnose the position and movement of mid- and upper-tropospheric features, including western disturbances.

Multiple satellite-based rainfall estimation products were evaluated: (1) Global Precipitation Measurement (GPM) Integrated Multisatellite Retrievals for GPM (IMERG) at 0.1° × 0.1° resolution; (2) IMD Daily Merged Satellite-Gauge product at 0.25° × 0.25° resolution; (3) Hydro-Estimator (HEM) using infrared brightness temperatures with NWP model augmentation; and (4) INSAT Multispectral Rainfall Algorithm (IMSRA) combining satellite observations with model-derived moisture fields at 0.25° × 0.25° resolution.

3.3. Numerical Weather Prediction Models

Forecast products from two operational NWP systems were analysed. The IMD Global Forecast System (IMD-GFS T-1534) is a global spectral model with approximately 12 km horizontal resolution, 64 hybrid sigma-pressure vertical levels, and a semi-Lagrangian dynamical core. Initial conditions are generated by the National Centre for Medium Range Weather Forecasting (NCMRWF) four-dimensional ensemble-variational data assimilation system (4DEnsVar), which assimilates conventional and satellite observations. The model produces 10-day forecasts initialized at 00, 06, 12, and 18 UTC.

The Weather Research and Forecasting (WRF) model was run at 3 km horizontal resolution with 45 vertical levels extending to 50 hPa, utilizing initial and boundary conditions from IMD-GFS.

The WRF configuration included explicit radiation, surface layer, and cumulus parameterization schemes appropriate for high-resolution applications. Both 240-hour GFS forecasts and 72-hour WRF forecasts were evaluated to assess the prediction skill at various lead times.

3.4. Thermodynamic Analysis

RS/RW measurements at 0000 UTC are utilized for calculation of standard thermodynamic indices viz. Showalter Index (SI), Lifted Index (LI), Severe Weather Threat Index (SWEAT), K-Index (KI), Total Totals Index (TTI), Convective Available Potential Energy (CAPE), Convective Inhibition (CIN), Level of Free Convection (LFC), Bulk Richardson Number (BRN), and Precipitable Water Content (PWC). These parameters provide quantitative measures of atmospheric stability, moisture availability, and convective potential (Doswell and Rasmussen, 1994; Singh & Thapliyal, 2022; Thapliyal & Singh, 2025).

4. Results and Discussion

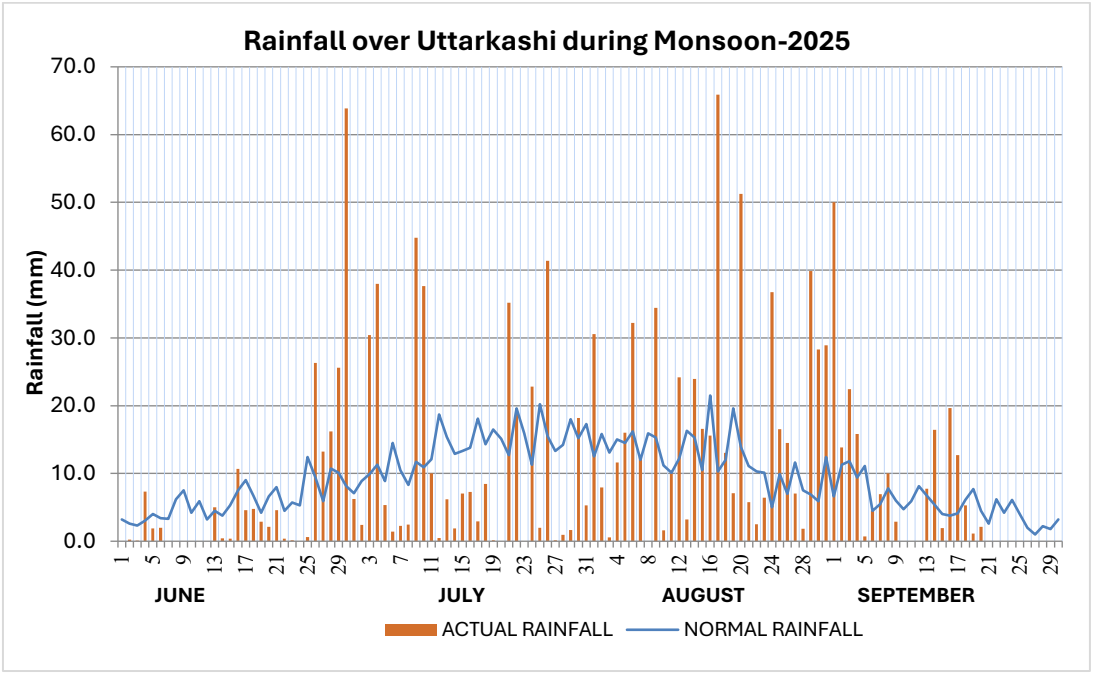
4.1. Large-Scale Climatic Background and Ocean-Atmosphere Interactions

The 2025 southwest monsoon season unfolded under a distinctive configuration of large-scale ocean-atmosphere conditions that significantly influenced monsoon rainfall patterns over the Indian subcontinent. El Niño-Southern Oscillation (ENSO) conditions remained neutral throughout the monsoon period (June-September 2025), with sea surface temperature anomalies in the Niño 3.4 region staying within ±0.5°C of the long-term mean. Similarly, the Indian Ocean Dipole (IOD) exhibited neutral conditions during the early monsoon months of June and July. However, a weak negative IOD phase developed during the late monsoon season (August-September), characterized by relatively warmer sea surface temperatures in the eastern equatorial Indian Ocean compared to the western basin. The combination of neutral ENSO and the evolution toward weak negative IOD conditions created a favourable large-scale environment for enhanced monsoon activity over the Western Himalayan region during August. Neutral ENSO conditions typically allow the monsoon system to be governed more directly by regional processes and intraseasonal oscillations rather than being strongly modulated by Pacific Ocean forcing (Kumar et al., 2006). The absence of El Niño conditions—which typically suppress Indian monsoon rainfall—allowed for unrestricted development of monsoon depressions and low-pressure systems, while the weak negative IOD phase developed late during the season. This favourable background state contributed to the observed excess monsoon rainfall across Uttarakhand (122% of LPA).

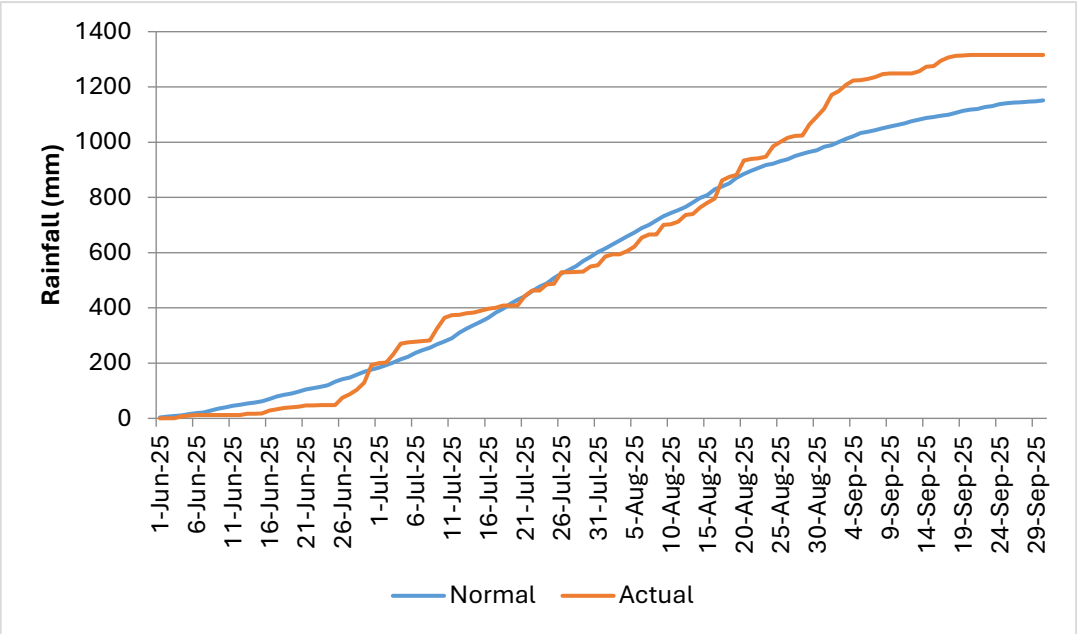
4.2. Monsoon 2025 Rainfall Characteristics over Uttarkashi

The southwest (SW) monsoon 2025 advanced into many parts of Uttarakhand on 20th June 2025 and covered the entire Uttarakhand State on 24th June 2025. Uttarakhand received 1420.5 mm of rainfall from June to September, representing 122% of the long-period average (LPA) of 1162.7 mm, categorizing the season as "excess". Uttarkashi district received 1315.8 mm of rainfall, corresponding to 115% of its LPA of 1151.2 mm.

The temporal evolution of cumulative rainfall showed considerable variability. The day-to-day comparison of the actual and normal rainfall of Uttarkashi district is shown in Fig. 3 (i), and the daily cumulative rainfall of Uttarkashi district is shown in Fig. 3(ii). The cumulative rainfall of Uttarkashi district was less than the LPA during the month of June; thereafter, the rainfall increased, and the cumulative rainfall became above normal and remained so during the first fortnight of July. During the second fortnight of July and the first fortnight of August, the cumulative rainfall remained below normal, and thereafter, in the second fortnight of August, it increased steeply, reaching 15% above LPA in September 2025.



(i)



(ii)

Fig 3: Daily actual and normal rainfall of (i) Uttarkashi district. (ii) Daily cumulative actual and normal rainfall over Uttarkashi district.

From June to September 2025, heavy or more rainfall events were reported on 14 days in Uttarkashi district. The distribution of heavy or more rainfall was isolated on 7 occasions, scattered on 5 occasions and fairly widespread on 2 occasions. The intensity of rainfall spells is calculated using AWS data based on the IMD criteria (ADGM(R), 2015). Two very intense spells (31-50 mm/hour) of rainfall were observed in Uttarkashi district in July and September.

4.3. Meteorological Conditions During August 3-6, 2025

The period leading up to the disaster was characterized by progressive intensification of monsoon activity over the Uttarkashi district. Very light to light rainfall was observed on August 3, increasing to very light to moderate rainfall on August 4 & 5. Fairly widespread moderate rainfall with heavy to very heavy amounts at isolated places was recorded over Uttarkashi district on 6th August, 2025, i.e., between 08:30 IST on 5th August and 08:30 IST on 6th August. The 24-hour accumulated rainfall reported at different stations in Uttarkashi district from 03rd to 06th August, 2025, is given in Table 1.

Rainfall observations from stations in the Uttarkashi district showed spatial heterogeneity. The stations closest to Dharali—the Harsil AWS and Harsil manual gauge—recorded 18.5 mm and 20.6 mm rainfall, respectively, on August 6 (accumulated from 08:30 IST August 5 to 08:30 IST August 6). Other stations in the district recorded higher accumulations. Figure 4 shows the spatial distribution of 24-hour accumulated rainfall over Uttarakhand recorded on August 06, 2025, and the star (black) shows the location of Dharali.

Table-1: Rainfall at different rain gauge stations in Uttarkashi district during 3-6 August 2025.

	Station	**03rd Aug**	**04th Aug**	**05thAug**	**06th Aug**
DRMS	Barkot	0.0	5.0	18.0	40.0
	Bhatwari	**0.0**	**30.0**	**10.0**	**46.0**
	Dunda	0.0	13.0	0.0	0.0
	Uttarkashi_cwc	0.8	8.2	27.0	41.4
	Uttarkashi	1.0	8.0	27.0	48.0
	Purola	2.0	15.0	12.0	50.0
	Mori	0	2.0	18.0	0.0
NON-DRMS	Chinalisayur	0	8.0	1.0	46.0
	Maneri	0.0	2.0	31.0	103.0
	Beef/Jan ki chatti	**0.0**	**27.0**	**9.6**	**138.0**
	Kuthnaur	10.0	12.0	10.0	78.0
	Harsil (CWC)	**0.0**	**0.0**	**6.2**	**20.6**
AWS	Sankri	8.0	34.0	16.0	52.0
	Gangotri	**1.0**	**-**	**-**	**3.0**
	Jan ki chatti	**0.5**	**14.5**	**28.5**	**42.0**
	Barkot	0.5	4.0	12.5	46.5
	Naugaon	0.0	14.0	16.5	50.0
	Harsil	**0.0**	**3.5**	**9.0**	**18.5**

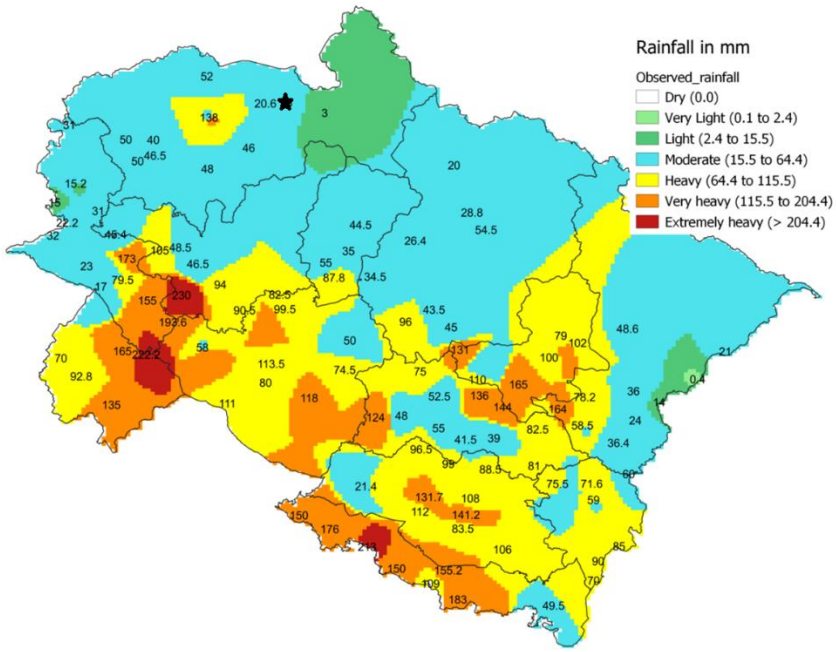


Fig 4: Twenty-four-hour accumulated rainfall recorded on the morning of 06th August 2025.

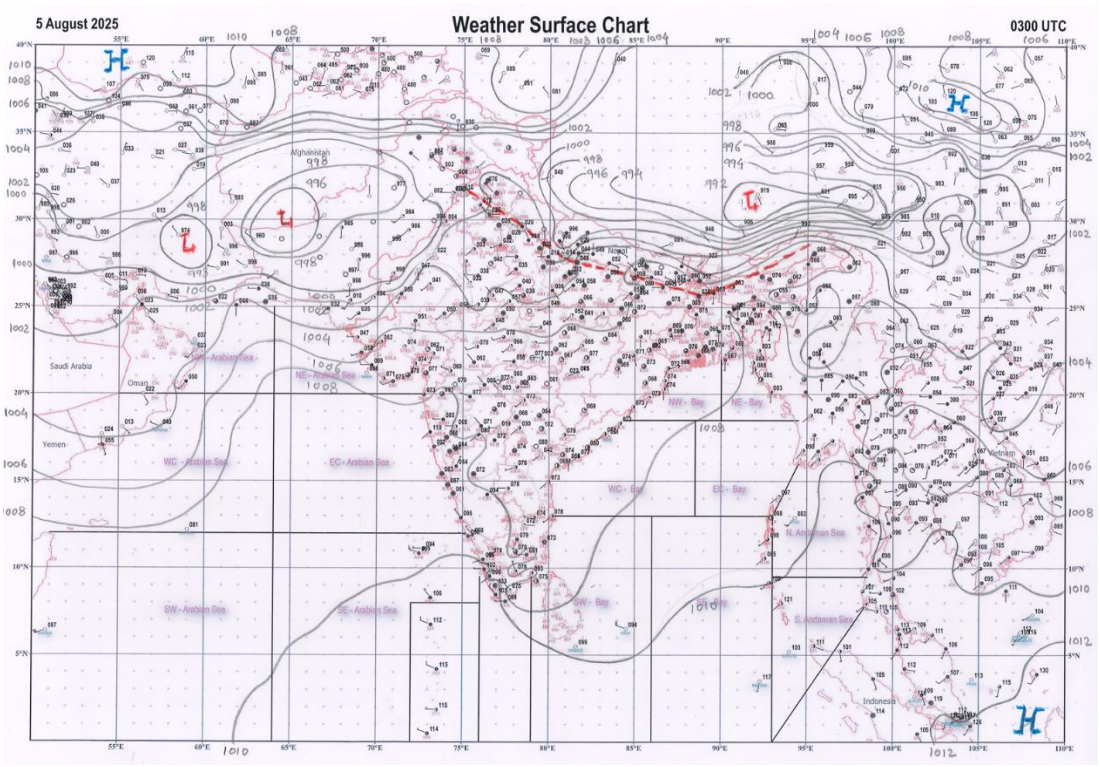
4.4. Synoptic-Scale Atmospheric Configuration

The large-scale atmospheric circulation pattern on August 5, 2025, featured several synoptically favourable elements for enhanced monsoon rainfall over the Himalayan region. The monsoon trough at mean sea level passed through Amritsar, Patiala, Muzaffarnagar, Kheri, and Valmik Nagar and then east–northeastwards to the Arunachal Pradesh close to foothills of the Himalayas on August 5, 2025 [Fig. 5(i)]. The western end of the monsoon trough shifted slightly southwards on August 6 and passed through Ferozepur, Karnal, Moradabad, Kheri, Jalpaiguri and then northeastward to the Arunachal Pradesh close to the foothills of the Himalayas.

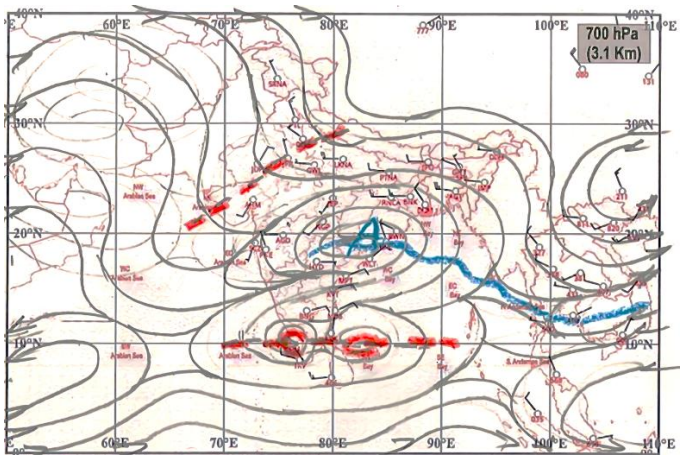
In the mid-troposphere (700 hPa level, approximately 3.1 km above mean sea level), a trough extended from northwest Uttar Pradesh to the northeast Arabian Sea across south Haryana, east Rajasthan, and Gujarat on August 5, 2025 [Fig. 5(ii)]. This feature persisted through August 6, although with a slight eastwards shift, running from central north Uttar Pradesh to northern Kutch between 3.1 and 4.5 km above mean sea level.

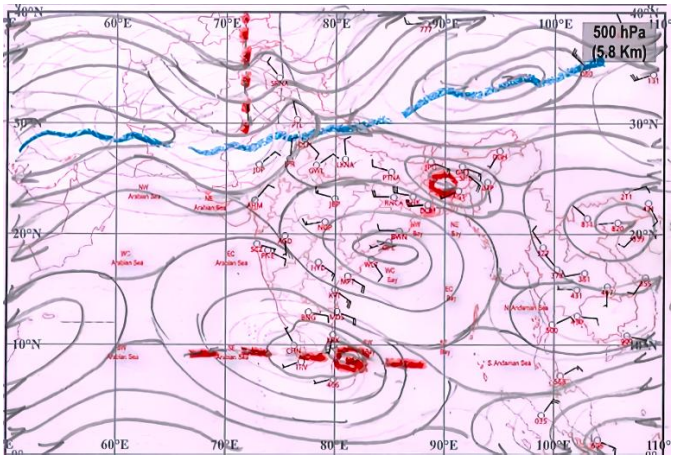
A particularly significant synoptic feature was the presence of a Western disturbance in the middle and upper troposphere. On August 5, Western Disturbance appeared as a trough in the middle troposphere with its axis at 5.8 km above mean sea level (approximately 500 hPa) oriented along 72°E to the north of 30°N 2025 [Fig. 5(iii)]. By August 6, this feature intensified into a cyclonic

circulation over Punjab and a neighborhood at 5.8 km, with an associated trough aloft at 7.6 km (near 400 hPa) along 73°E north of 32°N. Additionally, a low-level cyclonic circulation laid over Himachal Pradesh and adjoining Uttarakhand at 1.5 km above mean sea level on August 6.



(i)





(ii) (iii)

Fig 5: Analysed (i) 0300UTC 05th August surface chart, (ii) 0000UTC 05th August 700 hPa & (iii) 500 hPa level upper air charts. Red dashed lines depict troughs, blue zigzag lines depict ridges, C & A depict cyclonic and anticyclonic circulations, and L & H show areas of low and high pressure.

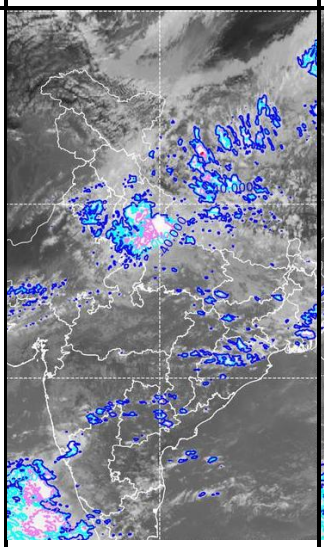
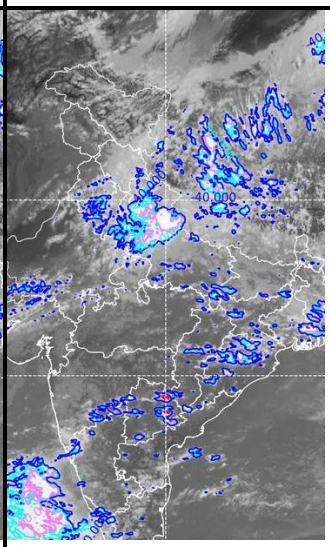
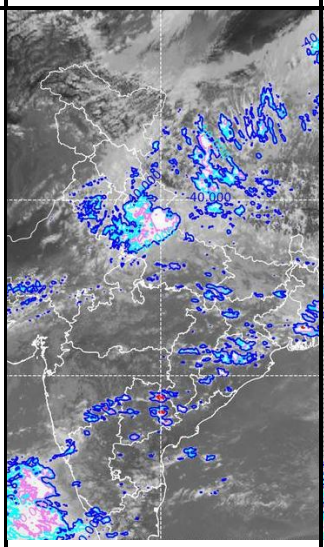
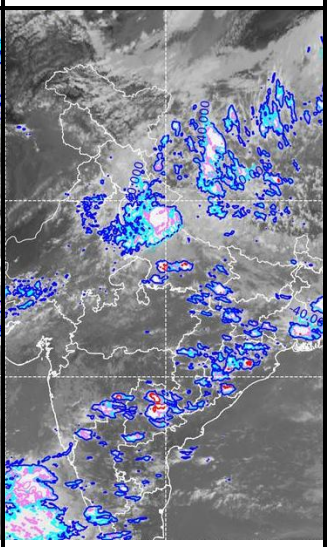
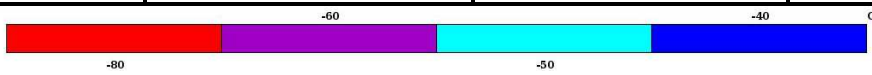
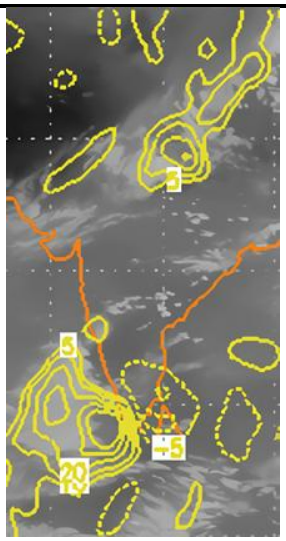
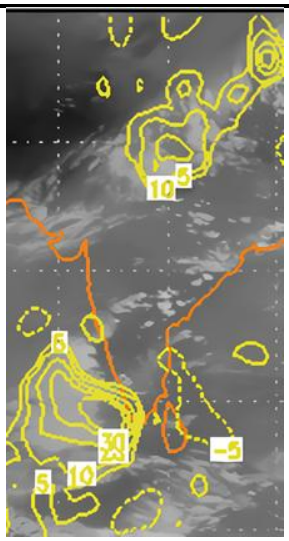
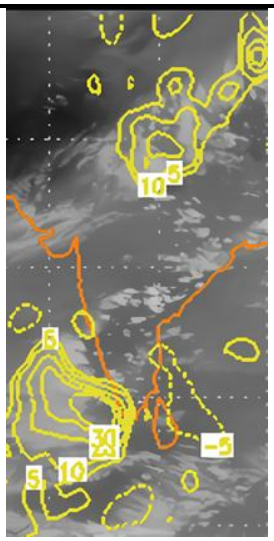
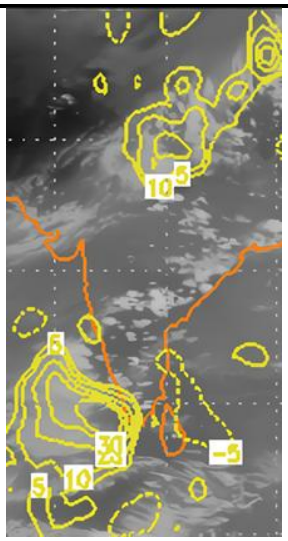
This synoptic configuration creates favourable dynamical conditions for the occurrence of extreme rainfall over the Himalayan region. The presence of the monsoon trough north of its normal position with the eastern end running close to the foothills provides low-level moisture convergence, while the mid-tropospheric trough supplies cyclonic vorticity and ascent. The western disturbance in the upper troposphere contributes to upper-level divergence and provides additional lift through positive vorticity advection. The quasistationary nature of these features allowed for prolonged forcing over the region (Dube et al., 2014; Rasmussen and Houze, 2012).

4.5. Satellite-derived Convective Structure and Atmospheric Kinematics

INSAT-3D imagery was analysed to study the characteristics of the precipitation-producing systems (Fig. 6). July and August are the wettest months for Uttarakhand, and more than 800 mm of rainfall, which is more than 50% of the total annual rainfall of Uttarakhand, is observed during these two months. Consequently, cloudiness is higher during these two months over Uttarakhand. The analysis of satellite images shows that most of Uttarakhand was covered with clouds from August 04 until the morning of August 06. However, the thick cloud mass and lowest cloud top brightness temperature (CTBT) of approximately -60°C was over the southern parts of Uttarakhand for most of the time during the period. The region with a CTBT of approximately -40 to -50°C extended up to the Uttarkashi district (Fig. 6).

The region of maximum low-level convergence (LLC) and upper-level divergence (ULD) was over Uttarakhand due to the presence of favourable synoptic systems from surface to middle-tropospheric levels. The region of maximum ULD shifted slightly north westwards during the 13:15 to 13:42 IST scan with a region of 5 to 10 × 10-5 s-1 divergence over the Uttarkashi district. However, the area of higher LLC decreased during the 13:15 to 13:42 IST scan with 5 × 10-5 s-1 convergence values over southern parts of Uttarakhand.

The thick cloud mass and area of the highest CTBT remained over the southern Uttarakhand region until the afternoon and shifted over the northern parts of Uttarakhand during the evening and nighttime on August 05. The satellite-derived water vapour winds (WVW) show the position of troughs in westerlies between 500-250 hPa levels roughly along Long. 72°E north of Lat.30°N. The trough in westerlies was almost stationary over the same region with very little fluctuation in the position on August 05, thus providing persistent large-scale ascent over the region. The quasistationary nature of this middle- and upper-level WD, the presence of a monsoon trough at lower levels and a slow-moving mid-tropospheric trough, created conditions favourable for a long-lived convective system and extreme rainfall accumulation over Uttarakhand (Lin et al., 2001).

Satellite Products	12:45 to 13:12 IST	13:15 to 13:42 IST	13:45 to 14:12 IST	14:15 to 14:42 IST
CTBT				
				
ULD				

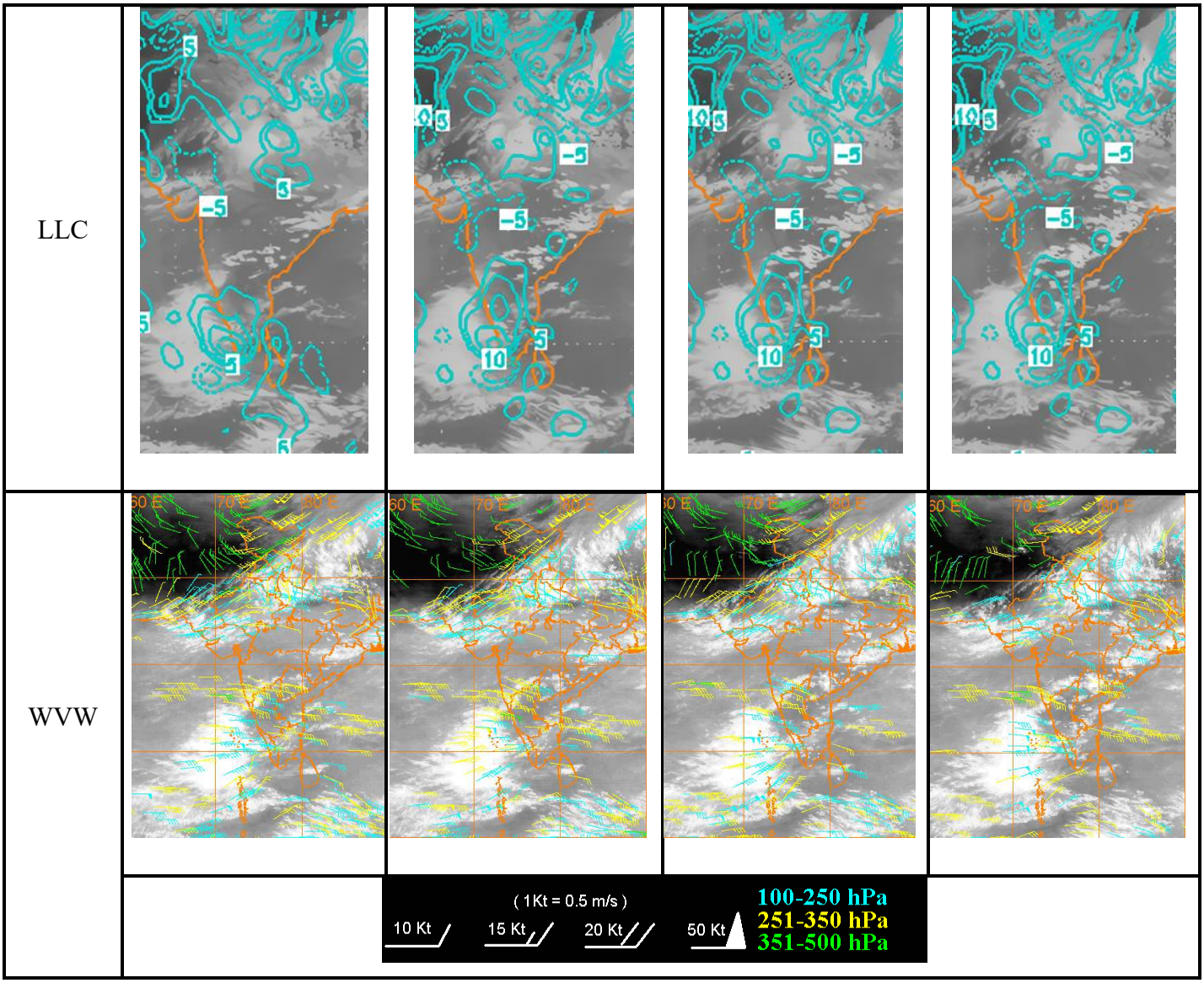


Fig 6: CTBT, ULD, LLC and WVW based on INSAT 3D from 12:45 to 14:42 IST on 05th August.

4.6. Quantitative Precipitation Estimation from Satellite Observations

The rainfall observed on August 05 from ground stations is compared with the rainfall estimates from different satellites and different estimation algorithms. The daily GPM IMERG rainfall at 0.1° X 0.1° and IMD Daily Merged Satellite Guage Rainfall at 0.25° X 0.25° spatial resolution are shown in Figure 7. The GPM and IMD show rainfall of 20 mm in and around the Dharali area. The GPM dataset shows an underestimation of rainfall, and the spatial position of the rainfall maxima does not align with the ground-based observations (Fig. 4). However, the IMD rainfall intensity and spatial distribution estimation are closer to ground-based observations.

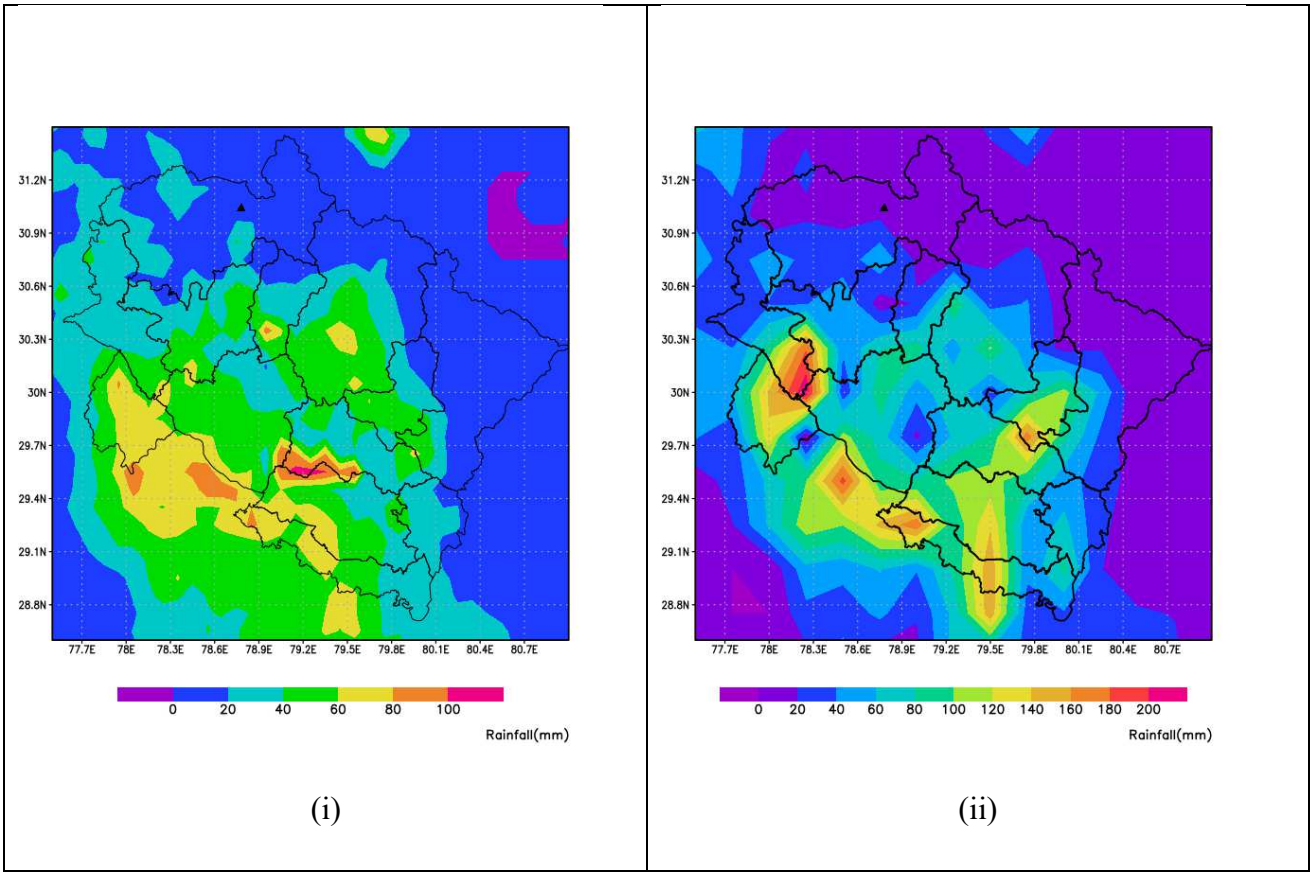


Fig 7: (i) The daily GPM IMERG rainfall at 0.1° and (ii) IMD Daily Merged Satellite Guage Rainfall at 0.25° spatial resolution. The black triangle is the location of Dharali in Uttarkashi.

Different high-resolution rainfall estimation techniques, such as the Hydro-Estimator (HEM) and Insat Multispectral Rainfall Algorithm (IMSRA), are utilized using INSAT 3D sensors. HEM primarily uses a 10.7-µm infrared channel for brightness temperatures to distinguish raining from nonraining areas and estimate rainfall rates, supplemented by numerical weather prediction model data to account for moisture availability, subcloud evaporation, thermodynamic profiles, and orographic effects. IMSRA derives rainfall by combining satellite observations (IR/WV BTs, TRMM microwave rainfall, and cloud information) with NWP-derived moisture fields. The algorithm calibrates satellite BTs with microwave rainfall, applies model-based corrections, and validates results using DWR and AWS measurements. Figure 8 shows the comparison of HEM- and IMSRA-based daily rainfall plots. The HEM shows 60 to 130 mm rainfall, while IMSRA shows 45 to 80 mm rainfall over the Uttarkashi district. The IMSRA underestimated the rainfall maxima, whereas the HEM overestimated the rainfall maxima, and the maxima of both estimations did not spatially align with ground observations (Fig. 4).

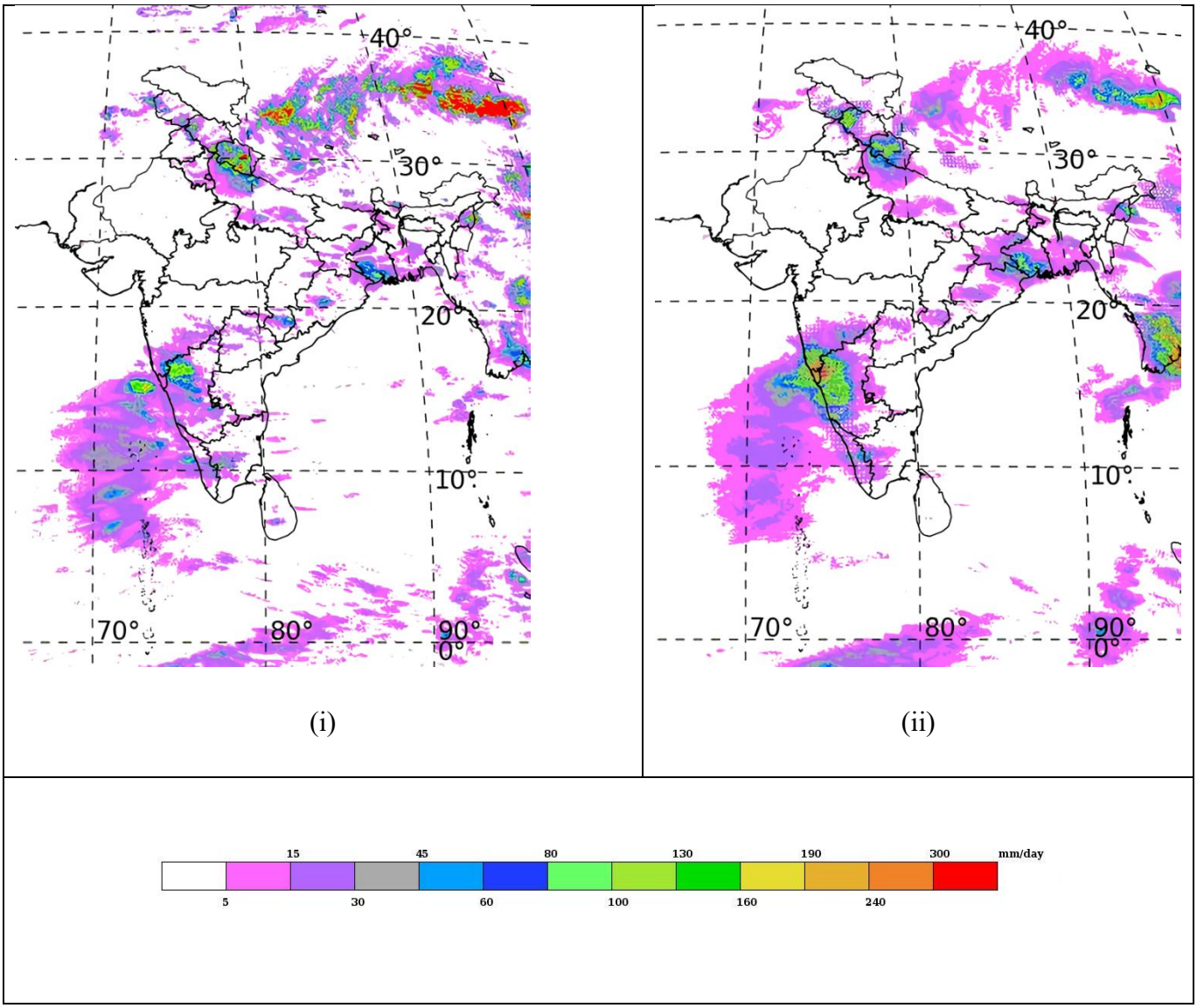


Fig 8: (i) HEM- and (ii) IMSRA-based daily rainfall plots for August 05, 2025.

A comparison of ground-based rainfall observations with satellite-derived estimates revealed substantial differences in both magnitude and spatial distribution. However, all these satellite estimations show rainfall maxima over southern parts of Uttarakhand, which is in agreement with the ground-based observations. There are persistent challenges in satellite-based rainfall estimation over complex terrain, as orographic effects influence both the relationship between cloud-top properties and surface rainfall (through seeder-feeder mechanisms and terrain-induced convergence) and the representativeness of radar reflectivity measurements (Houze, 2012; Kirshbaum et al., 2018). Warm rain processes, which are more common in orographic

precipitation, are particularly difficult to detect from infrared and passive microwave sensors (Shige et al., 2013).

4.7. Thermodynamic analysis

Various thermodynamic indices have been calculated based on 0000UTC RS/RW data from the Patiala station, which is the closest station to Uttarkashi, to investigate the stability and evolution of upper-atmospheric conditions. The skew-t plot of August 04 & 05 and various indices are shown in Table 2. The skew-t plot shows higher moisture content at lower and upper tropospheric levels and relatively lower moisture at middle tropospheric levels on August 04. The moisture at middle tropospheric levels increased on 05th August, thereby making higher moisture throughout the air column. This resulted in an increase in precipitable water for the entire sounding from 60 mm on August 04 to 69 mm on August 05.

Most of the thermodynamic indices, such as the Showalter Index, SWEAT Index, K Index and Totals Totals Index, suggested slightly increased atmospheric instability on 05th August compared to 04th August. The Showalter Index decreased from -0.28 to -1.56 (more negative values indicate greater instability), while the K-Index increased from 38.6 to 42.3 and the Total Totals Index from 41.4 to 44.0. The SWEAT index, which combines vertical wind shear with thermodynamic instability, increased from 257.59 to 264.61, suggesting favourable conditions for organized convection.

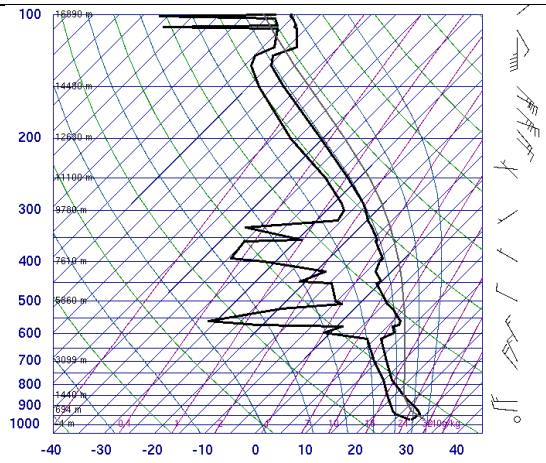
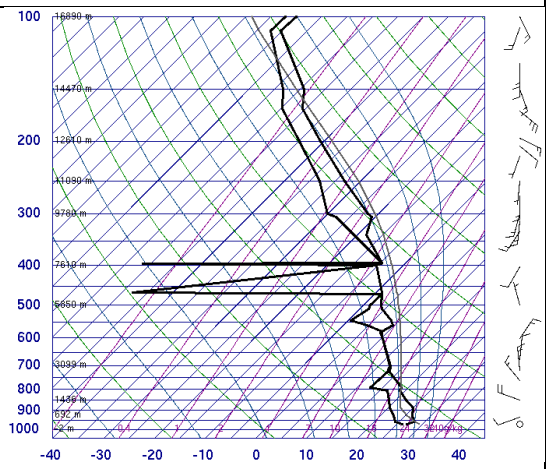
The bulk Richardson number (BRN) decreased to half on 05th August, suggesting increased dynamical instability on 05th August. There was a significant reduction in convective available potential energy (CAPE) and convective inhibition (CIN) values on 05th August and a marginal reduction in the lifted index. Overall, the daily evolution of thermodynamic parameters suggests an increase in thermodynamic and dynamic instability on 05th August 2025.

Interestingly, convective available potential energy (CAPE) decreased substantially from 2145 J/kg on August 4 to 1097 J/kg on August 5, while convective inhibition (CIN) increased (in magnitude) from -25.58 J/kg to -52.54 J/kg. The level of free convection increased from 850 hPa to 813 hPa. These changes suggest that while buoyant energy decreased, the atmosphere became more easily triggered due to increased low-level moisture and saturation.

The bulk Richardson number, which relates buoyant energy to vertical wind shear, decreased from 267 to 125, indicating enhanced potential for organized convective systems. This combination of reduced CAPE but increased moisture, higher lifting potential, and favourable dynamic forcing is

characteristic of monsoon convection over northern India, where high-CAPE environments are less common than in other tropical regions, yet intense precipitation systems frequently develop (Romatschke and Houze, 2011).

Table 2: Various thermodynamic indices and skew-t plot based on 0000 UTC of 04th and 05th August RS/RW data of Patiala station.

Index/parameter	**04th August 2025 at 0000UTC**	**05th August 2025 at 0000UTC**
Skew-t		
SI	-0.28	-1.56
LI	-3.62	-3.44
SWEAT index	257.59	264.61
KI	38.6	42.3
TTI	41.4	44
CAPE(J/kg)	2145.02	1096.63
CIN(J/kg)	-25.58	-52.54
LFC (hPa)	850.49	813.46
BRN	267.03	124.99
PWC (mm)	60.03	68.89

4.8. Numerical Weather Prediction Model Performance

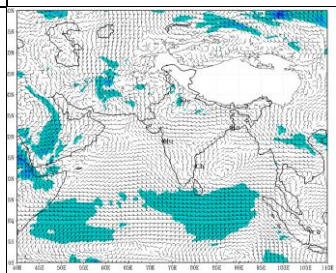
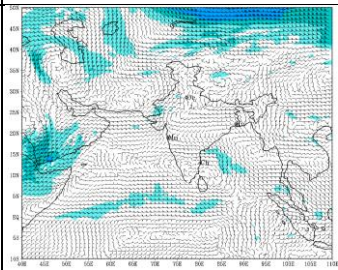
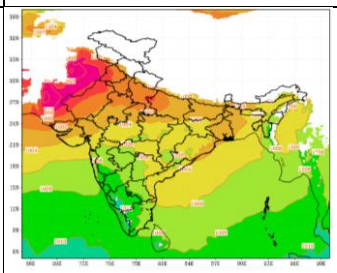
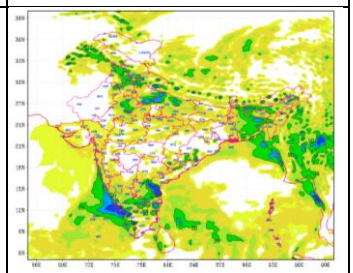
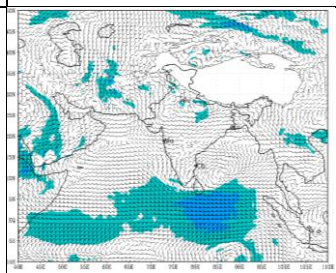
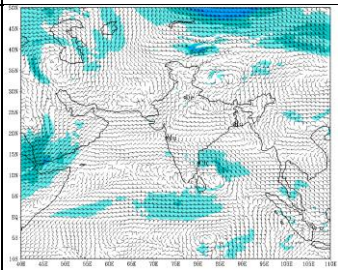
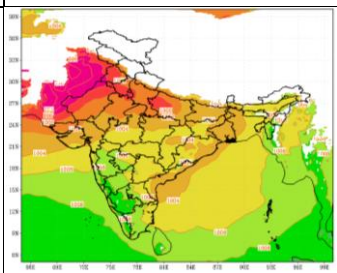
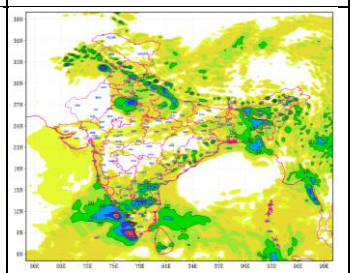
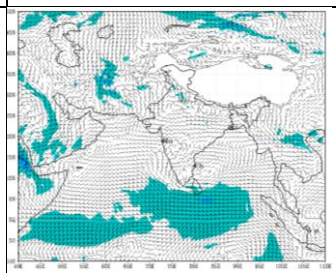
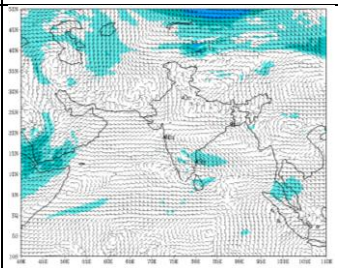
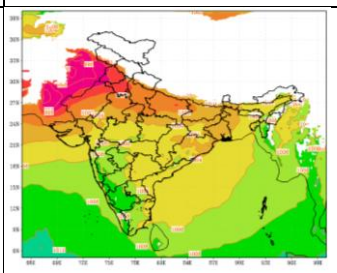
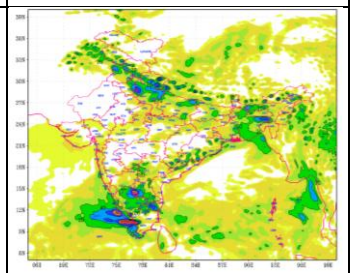
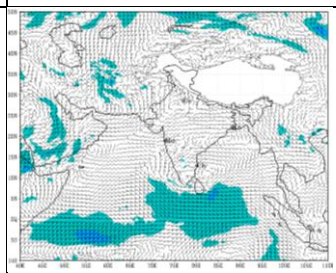
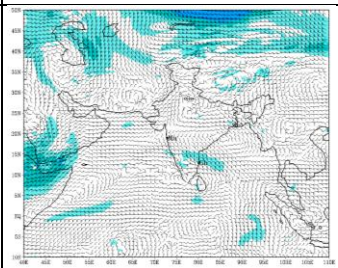
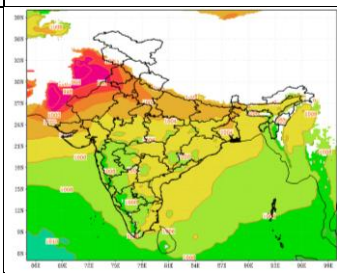
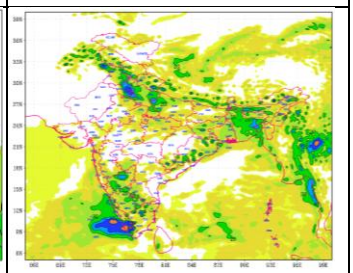
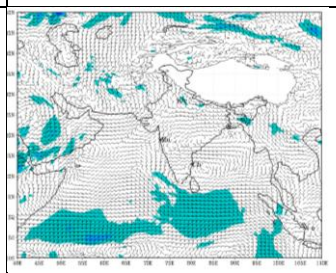
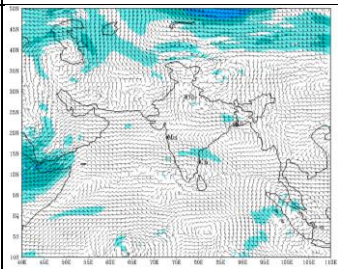
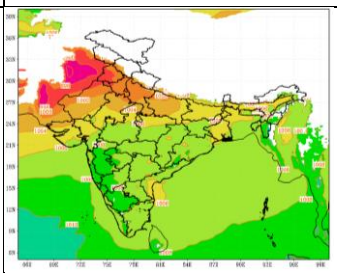
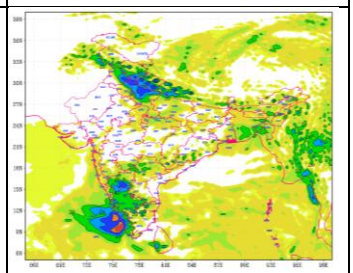
Evaluation of IMD-GFS forecasts initialized from August 1-5 (providing lead times of 1-5 days) showed reasonable skill in predicting the general synoptic configuration but varying success in rainfall forecasting. The model consistently predicted the monsoon trough at mean sea level, although with varying accuracy in position—some runs placed it slightly south of the observed location. The mid-tropospheric trough from northwest Uttar Pradesh to the northeast Arabian Sea was successfully forecast at lead times up to 5 days. Figure 8 shows IMD-GFS model forecasts for August 5, 2025, initialized from August 1-5 (providing 1-5 day lead times). Each row displays a different forecast run, with columns showing 700 hPa winds, 500 hPa winds, mean sea level pressure (MSLP), and 24-hour accumulated rainfall.

However, representation of the western disturbance at 500 hPa was challenging across most forecast runs—the feature was either very weak or entirely absent in the forecasts. This atmospheric feature is significant because the upper-level forcing provided by the western disturbance is crucial for organizing and intensifying monsoon precipitation over northern India (Hunt et al., 2018).

Precipitation forecasts from GFS showed considerable run-to-run variability. The forecasts initialized on August 3 and August 5 performed best, predicting very heavy rainfall (>130 mm) at some locations in Uttarakhand. These runs forecast heavy rainfall (40-70 mm) over isolated areas of Uttarkashi district, reasonably capturing the observed precipitation distribution.

Figure 9 presents the WRF model forecasts for August 5, 2025, initialized from August 3-5 (providing 1-3 day lead times). The layout mirrors Figure 8, displaying 700 hPa winds, 500 hPa winds, MSLP, and 24-hour accumulated rainfall for each forecast run. The WRF model at a 3 km resolution showed systematic biases in its analysis and forecasts. Similar to GFS, WRF successfully predicted the mid-tropospheric trough but struggled to represent the western disturbance at 500 hPa. WRF precipitation forecasts generally predicted moderate rainfall (20-40 mm) over Uttarakhand from the August 3 and August 5 initializations, with rainfall maxima displaced over Uttar Pradesh. The August 4 initialization performed better for Uttarkashi specifically, predicting heavy rainfall (40-70 mm). Overall, WRF showed less skill than GFS in this case, possibly due to its dependence on GFS for initial and boundary conditions combined with its own systematic biases.

Both models showed rainfall maxima over southern Uttarakhand and adjoining Uttar Pradesh and provided fairly good forecasts of heavy to very heavy rainfall with a lead time of 3 to 5 days.

Forecast for 05th August based on	700 hPa wind	500 hPa wind	MSLP	Rainfall
01.08.2025				
02.08.2025				
03.08.2025				
04.08.2025				
05.08.2025				

Legends				

Fig. 9: GFS model-based forecast and analysed winds at 700 hPa and 500 hPa levels, MSLP and predicted rainfall based on 0000 UTC from 01st to 05th August 2025.

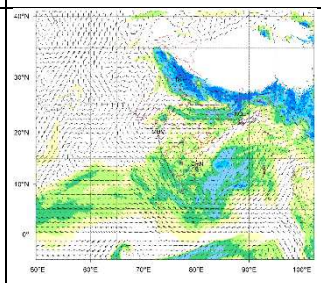
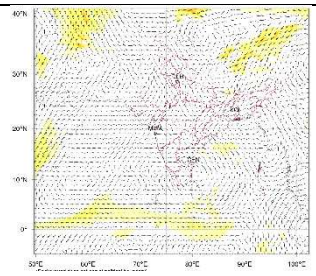
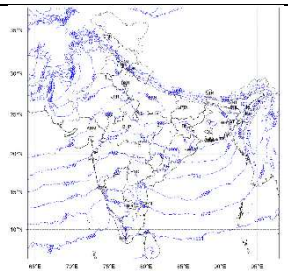
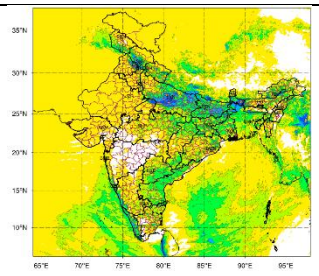
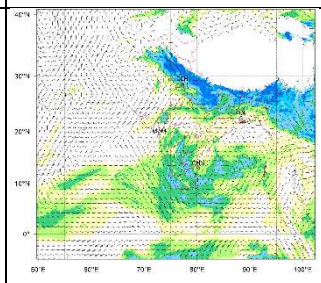
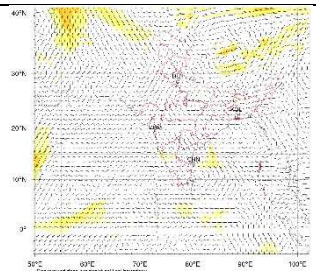
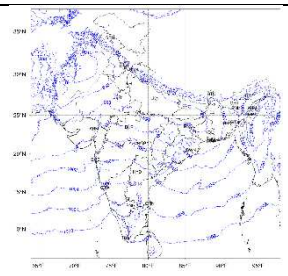
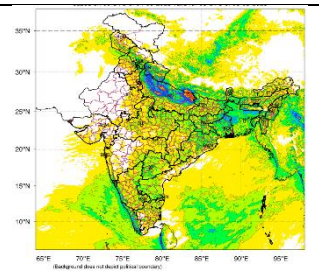
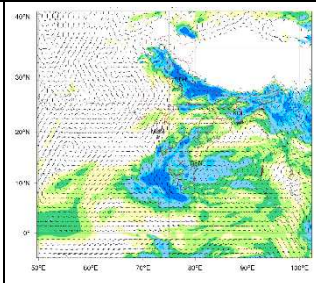
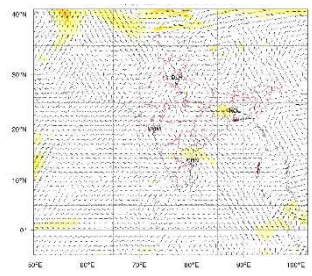
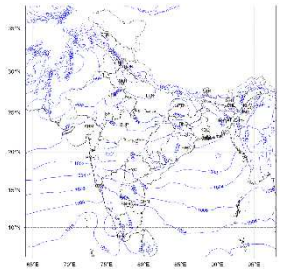
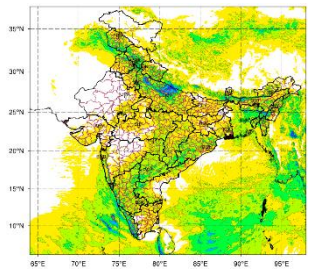
Forecast for 05th August based on	700 hPa wind	500 hPa wind	MSLP	Rainfall
03.08.2025				
04.08.2025				
05.08.2025				
Legends				

Fig 10: WRF model-based forecast and analysed winds at 700 hPa and 500 hPa levels, MSLP and predicted rainfall based on 0000 UTC from 03rd to 05th August 2025.

5. Conclusions

The analysis of multisource rainfall datasets—including manual rain gauges, AWS observations, satellite, and merged satellite–gauge rainfall estimates—show that the Dharali–Harsil region received moderate (~20 mm) rainfall on 05th August 2025. Very heavy to extremely heavy rainfall was recorded over the southern districts of Uttarakhand, where deep convective cloud bands with cloud-top temperatures below –60°C persisted throughout the day. Satellite products and thermodynamic diagnostics indicate that although deep convection and the strongest moisture convergence remained anchored over southern Uttarakhand, the broader synoptic setting—an active monsoon trough, mid-tropospheric cyclonic circulations, and a stationary trough in westerlies—created a moist and dynamically unstable environment extending into Uttarkashi district.

Despite the absence of extremely heavy rainfall over Dharali, the event triggered a destructive debris avalanche. This highlights the sensitivity of high-altitude Himalayan slopes, where unconsolidated glacial deposits, steep terrain, high antecedent moisture, and ongoing cryosphere changes create conditions where moderate rainfall can exceed critical thresholds for failure. Thermodynamic analysis indicated increased column moisture, higher precipitable water, and enhanced dynamic instability on 5th August, despite a reduction in CAPE, suggesting a moist, saturated, and weakly buoyant environment favourable for intense monsoon convection over complex terrain. The findings underscore that in the Higher Himalayas, the rainfall threshold for slope failure is significantly lower than that in the middle or southern Himalayan regions.

Evaluation of different rainfall estimation techniques and algorithms showed the rainfall maxima over southern Uttarakhand and adjoining Uttar Pradesh. However, there are some notable uncertainties, such as GPM underestimating rainfall intensity, IMSRA underestimating maxima, and HEM overestimating amounts and misplacing spatial peaks. These discrepancies reflect fundamental challenges in remote sensing of orographic precipitation and highlight the continued importance of dense ground observation networks. Among the estimation techniques evaluated, the IMD Daily Merged Satellite-Gauge product performed best by leveraging both satellite and ground observations.

Numerical weather prediction model evaluation revealed that while both IMD-GFS and WRF successfully captured the broad synoptic environment, significant deficiencies existed in the representation of the upper-level western disturbance and in the localization of precipitation maxima. The GFS model showed better overall performance than WRF and successfully predicted heavy to very heavy rainfall over Uttarakhand at 3-5 day lead times in some forecast runs.

However, the inability to consistently predict the precise location and intensity of rainfall maxima remains a critical limitation for these models.

Overall, the study demonstrates that extreme events in the Uttarakhand Himalaya are driven by multiscale interactions—monsoon trough position, embedded western disturbances, deep moisture availability, mesoscale convergence, and orographic enhancement. The findings highlight the need for improved high-resolution rainfall estimation, more accurate representation of mid-level dynamics, and enhanced nowcasting systems to provide timely warnings for highly localized hydrometeorological hazards in the Himalayan region. The August 2025 Dharali disaster exemplifies the multiscale complexity of Himalayan hydrometeorological hazards, where large-scale atmospheric circulation, mesoscale convective organization, local orographic enhancement, and geomorphological sensitivity interact to produce catastrophic outcomes. As climate change continues to alter both atmospheric circulation patterns and mountain cryosphere stability, improved understanding and prediction of such events becomes increasingly urgent for protecting vulnerable Himalayan communities.

Acknowledgements

The authors acknowledge the India Meteorological Department for providing observational data, model forecasts, and satellite products. We also acknowledge the District Administration of Uttarkashi and emergency responders for their efforts during this disaster. The views expressed in this paper are those of the authors and do not necessarily represent the official policy of the India Meteorological Department or Ministry of Earth Sciences.

References

Allen, S.K., Rastner, P., Arora, M., Huggel, C., and Stoffel, M. (2016). Lake outburst and debris flow disaster at Kedarnath, June 2013: hydrometeorological triggering and topographic predisposition. Landslides, 13(6), 1479-1491. https://doi.org/10.1007/s10346-015-0584-3

Chevuturi, A., Dimri, A.P., and Thayyen, R.J. (2015). Climate change over Leh (Ladakh), India. Theoretical and Applied Climatology, 131(1-2), 531-545. https://doi.org/10.1007/s00704-016-1989-1

Dikshit, A., Sarkar, R., Pradhan, B., Acharya, S., & Dorji, K. (2019). Estimating Rainfall Thresholds for Landslide Occurrence in the Bhutan Himalayas. Water, 11(8), 1616. https://doi.org/10.3390/w11081616

Dikshit, A., Sarkar, R., Pradhan, B., Segoni, S., & Alamri, A. M. (2020). Rainfall Induced Landslide Studies in Indian Himalayan Region: A Critical Review. *Applied Sciences*, *10*(7), 2466. https://doi.org/10.3390/app10072466

Dimri, A.P. and Chevuturi, A. (2014). Model sensitivity analysis study for western disturbances over the Himalayas. Meteorology and Atmospheric Physics, 123(3-4), 155-180. https://doi.org/10.1007/s00703-013-0302-4

Dimri, A.P., Kumar, D., Choudhary, A., and Maharana, P. (2018). Future changes over the Himalayas: Mean temperature. -090, 199, 103446. https://doi.org/10.1016/j.gloplacha.2018.01.014

Doswell III, C.A. and Rasmussen, E.N. (1994). The effect of neglecting the virtual temperature correction on CAPE calculations. Weather and Forecasting, 9(4), 625-629. https://doi.org/10.1175/1520-0434(1994)009<0625:TEONTV>2.0.CO;2

Dube, A., Ashrit, R., Ashish, A., Sharma, K., Iyengar, G.R., Rajagopal, E.N., and Basu, S. (2014). Forecasting the heavy rainfall during Himalayan flooding—June 2013. Weather and Climate Extremes, 4, 22-34. https://doi.org/10.1016/j.wace.2014.03.004

Guzzetti, F., Peruccacci, S., Rossi, M., and Stark, C.P. (2008). The rainfall intensity–duration control of shallow landslides and debris flows: an update. Landslides, 5(1), 3-17. https://doi.org/10.1007/s10346-007-0112-1

Houze Jr, R.A. (2012). Orographic effects on precipitating clouds. Reviews of Geophysics, 50(1), RG1001. https://doi.org/10.1029/2011RG000365

Huggel, C., Clague, J.J., and Korup, O. (2012). Is climate change responsible for changing landslide activity in high mountains? Earth Surface Processes and Landforms, 37(1), 77-91. https://doi.org/10.1002/esp.2223

Hunt, K.M., Turner, A.G., and Shaffrey, L.C. (2018). The evolution, seasonality and impacts of western disturbances. Quarterly Journal of the Royal Meteorological Society, 144(710), 278-290. https://doi.org/10.1002/qj.3200

India Meteorological Department (2023). Climate of Uttarakhand. IMD Pune, Technical Report.

Iverson, R.M., Reid, M.E., Iverson, N.R., LaHusen, R.G., Logan, M., Mann, J.E., and Brien, D.L. (2000). Acute sensitivity of landslide rates to initial soil porosity. Science, 290(5491), 513-516. https://doi.org/10.1126/science.290.5491.513

Jones, P., Thomas, C., Peterson, T., Parker, D., Thigpen, R., and Bojinski, S. (2010). Guide to the GCOS Surface Network (GSN) And GCOS Upper-Air Network (GUAN) (2010 update of GCOS-73). World Meteorological Organization, Geneva. Retrieved from https://library.wmo.int/doc_num.php?explnum_id=3855,3

Kidd, C. and Levizzani, V. (2011). Status of satellite precipitation retrievals. Hydrology and Earth System Sciences, 15(4), 1109-1116. https://doi.org/10.5194/hess-15-1109-2011

Kirshbaum, D.J., Adler, B., Kalthoff, N., Barthlott, C., and Serafin, S. (2018). Moist orographic convection: Physical mechanisms and links to surface-exchange processes. Atmosphere, 9(3), 80.https://doi.org/10.3390/atmos9030080

Lin, Y.-L., Chiao, S., Wang, T.-A., Kaplan, M.L., and Weglarz, R.P. (2001). Some common ingredients for heavy orographic rainfall. Weather and Forecasting, 16(6), 633-660.https://doi.org/10.1175/1520-0434(2001)016<0633:SCIFHO>2.0.CO;2

Martha, T.R., Roy, P., Jain, N., Khanna, K., Mrinalni, K., Kumar, K.V., and Rao, P.V.N. (2021). Geospatial landslide inventory of India—an insight into occurrence and exposure on a national scale. Landslides, 18(6), 2125-2141. https://doi.org/10.1007/s10346-021-01645-1

National Remote Sensing Centre (NRSC) (2025). Indian Satellite data based analysis of the Dharali Flash Flood. NRSC, ISRO. Retrieved from https://www.isro.gov.in/indian_satellite_data_based_analysis_of_the_dharali_flash_flood.html

Norris, J., Carvalho, L.M.V., Jones, C., and Cannon, F. (2014). WRF simulations of two extreme snowfall events associated with contrasting extratropical cyclones over the western and central Himalaya. Journal of Geophysical Research: Atmospheres, 119(7), 3945-3973. https://doi.org/10.1002/2014JD022592

Rasmussen, K.L. and Houze Jr, R.A. (2012). A flash-flooding storm at the steep edge of high terrain: Disaster in the Himalayas. Bulletin of the American Meteorological Society, 93(11), 1713-1724. https://doi.org/10.1175/BAMS-D-11-00236.1

Romatschke, U. and Houze Jr, R.A. (2011). Characteristics of precipitating convective systems in the South Asian monsoon. Journal of Hydrometeorology, 12(1), 3-26. https://doi.org/10.1175/2010JHM1289.1

Shige, S., Yamamoto, T., and Tsukiyama, T. (2013). Improvement of TMI rain retrievals in mountainous areas. Journal of Applied Meteorology and Climatology, 52(1), 242-254. https://doi.org/10.1175/JAMC-D-12-074.1

Stoffel, M. and Huggel, C. (2012). Effects of climate change on mass movements in mountain environments. Progress in Physical Geography, 36(3), 421-439. https://doi.org/10.1177/0309133312441010

Wieczorek, G.F., Larsen, M.C., Eaton, L.S., Morgan, B.A., and Blair, J.L. (2001). Debris-flow and flooding hazards associated with the December 1999 storm in coastal Venezuela and strategies for mitigation. US Geological Survey Open File Report, 1-31. https://doi.org/10.3133/ofr01144

Kumar, K.K., Rajagopalan, B., Hoerling, M., Bates, G., and Cane, M. (2006). Unravelling the mystery of Indian monsoon failure during El Niño. Science, 314(5796), 115-119. https://doi.org/10.1126/science.1131152

ADGM(R),2015,"Forecasting Circular No. 5/2015 (3.7)", ADGM(R)/UOI No. W-969, 7

Thapliyal, R., & Singh, B. (2023). A case study of exceptionally heavy rainfall event over Uttarakhand, India on 18th October, 2021 and its forecasting. Mausam, 74(3), 717-740, https://doi.org/10.54302/mausam.v74i3.4754

Karki, R., ul Hasson, S., Gerlitz, L., Talchabhadel, R., Schenk, E., Schickhoff, U., Scholten, T. and Böhner, J. (2018). WRF-based simulation of an extreme precipitation event over the Central Himalayas: Atmospheric mechanisms and their representation by microphysics parameterization schemes. Atmospheric Research, 214, 21-35. https://doi.org/10.1016/j.atmosres.2018.07.016

Singh, B., & Thapliyal, R. (2022). Cloudburst events observed over Uttarakhand during monsoon season 2017 and their analysis. *Mausam*, *73*(1), 91-104. https://doi.org/10.54302/mausam.v73i1.5084

Thapliyal, R., & Singh, B. (2025). Objective method for hailstorm forecasting over Dehradun, Uttarakhand, India. *Discover Atmosphere*, *3*(1), 28. https://doi.org/10.1007/s44292-025-00047-5

570